Available online at www.sciencedirect.com
ScienceDirect
Enzyme and Microbial Technology 39 (2006) 1347–1353
ENZYME AND MICROBIAL TECHNOLOGY
www.elsevier.com/locate/emt

The use of genome scale metabolic flux variability analysis for process feed formulation based on an investigation of the effects of the *zwf* mutation on antibiotic production in *Streptomyces coelicolor*

Michael E. Bushell [a,*], Susana I.P. Sequeira [a], Chiraphan Khannapho [a], Hongjuan Zhao [a], Keith F. Chater [b], Michael J. Butler [b], Andrzej M. Kierzek [a], Claudio A. Avignone-Rossa [a]

[a] *Microbial Science Group, School of Biomedical and Molecular Sciences, University of Surrey, Guildford, Surrey GU2 7XH, United Kingdom*
[b] *Department of Molecular Microbiology, John Innes Centre, Norwich Research Park, Colney, Norwich NR4 7UH, United Kingdom*

Received 3 May 2006; received in revised form 12 June 2006; accepted 14 June 2006

Abstract

Deletion of either of the genes (*zwf*), coding for glucose-6-phosphate dehydrogenase isoforms in *Streptomyces coelicolor*, resulted in an increase in *in vitro* determined glucose-6-phosphate dehydrogenase activity in the surviving isoform. Mutants carrying either one of these deletions exhibited significantly increased actinorhodin biosynthesis, an effect that was not predicted by simple flux balance simulation. The flux variability distribution, obtained using experimental measured variables as constraints, was examined. The reactions whose flux variabilities were most significantly affected, as a result of the increased actinorhodin production and changes in nutrient uptake rates, included reactions from a number of different pathways. These could be connected together to form an actinorhodin-generating network. They included glutamate synthesising and catabolising reactions. Subsequent experiments, in which glutamate was fed to steady state cultures, resulted in increased actinorhodin production and the *in silico* model predicted the importance of the same reactions that were amplified in the *zwf* model. Introduction of a constitutively expressed copy of *actII-orf4,* the pathway-specific activator of the actinorhodin pathway genes, on the integrating plasmid pIJ8714 resulted in a switch from growth dissociated (typical secondary metabolite) to growth associated antibiotic production.

Keywords: Flux variability analysis; Actinorhodin; Streptomyces; Antibiotic production; Antibiotic biosynthesis; *Streptomyces coelicolor*

1. Introduction

Several genome scale metabolic networks have been constructed for microbial species allowing *in silico* modelling of metabolic pathway activity [1]. Using such networks, quantitative simulation of microbial metabolism can be carried out using flux balance analysis (FBA). FBA modelling is a "constraint-based" approach that makes the assumption that metabolic network fluxes will reach a steady state, constrained by the stoichiometry of the network [2]. Despite this method resulting in an initially underdetermined system, a bounded solution space, containing all feasible fluxes within the network can be computed [3]. The solution space can be reduced further by specifying maximum and minimum fluxes through any particular reaction and then further refined by adding experimental data or examining responses to the imposition of hypothetical reaction fluxes [3].

The publication of the *Streptomyces coelicolor* genome sequence [4] has allowed the construction of a genome scale metabolic network for the species, providing the framework for FBA simulation of a *Streptomyces* [5].

Promising results have been obtained when applying a form of optimised flux balance analysis [6] to comparatively small networks for process design for a number of bioproducts, including production of recombinant DNA for gene therapy [7] and antibiotic yield optimisation [8]. In the latter, amino acid culture feeds were devised on the basis of hypotheses, generated by simulations involving a 57 reaction *in silico* pathway flux simulation of *Streptomyces clavuligerus* metabolism. This approach also provided hypotheses accounting for differential antibiotic production, depending on the identity of the growth limiting nutrient [9].In this study, we employ the concept of flux variability analy-

* Corresponding author.
E-mail address: m.bushel@surrey.ac.uk (M.E. Bushell).

0141-0229/$ – see front matter © 2006 Elsevier Inc. All rights reserved.
doi:10.1016/j.enzmictec.2006.06.011

sis [10] to highlight areas of metabolism from different pathways that can be connected to form an actinorhodin-generating network.

2. Materials and methods

2.1. Strains and culture media

All *S. coelicolor* strains were derived from M510 [11], itself a derivative of M145, the prototrophic strain used as the source of DNA for the sequencing of the genome of *S. coelicolor* A3(2) [4]. M510 differs from M145 only in the deletion of *redD*, the pathway-specific activator of genes for the biosynthesis of the red pigment undecylprodigiosin. Null mutations of *zwf* genes were made in M510 using in-frame deletions, exactly as previously described for *zwf* mutants of the closely related organism *Streptomyces lividans* 66 (which had been made using *S. coelicolor* genomic DNA: [11]). We engineered in-frame deletions of each of two *zwf* genes (*zwf1* and *zwf2*), encoding glucose-6-phosphate dehydrogenase isoforms. These are located within the two gene clusters encoding the pentose phosphate pathway enzymes in *S. coelicolor* A3(2), (http://www.sanger.ac.uk/Projects/S_coelicolor/; accession numbers AL031107 and AL096839). The *zwf1* deletion removed 1113 bp, to give a gene product retaining 195 amino acids from the N-terminus and 23 from the C-terminus; and the *zwf2* deletion replaced 612 bp with a 6-bp hybrid *Bam*HI-*Bgl*II site, to give a gene product retaining 29 amino acids from the N-terminus and 273 from the C-terminus. Strains were engineered to overproduce the enzymes of actinorhodin biosynthesis by the introduction of a constitutively expressed copy of *actII-orf4*, the pathway-specific activator of the actinorhodin pathway genes, on the integrating plasmid pIJ8714. The key features of pIJ8714 are: it is based on pSET152 [11,13], a plasmid that can replicate in *Escherichia coli*, be transferred by conjugation into *S. coelicolor*, and integrate efficiently and stably into the *S. coelicolor* chromosome at the φC31 prophage attachment site; and it contains a copy of *actII-orf4* under the control of the strong constitutive promoter *ermEp** [11].

The chemically defined (phosphate limited) bioreactor medium contained the following major nutrients (mM in reverse osmosis purified water): glucose, 194; citric acid, 2; $(NH_4)_2SO_4$, 50; Na_2HPO_4, 4 (3 for chemostat cultures); KCl, 10; $MgCl_2$, 1.25; Na_2SO_4, 2; $CaCl_2$, 0.25 and 5 ml per litre of the following trace components (mM): ZnO, 50; $FeCl_3$, 20; $MnCl_2$, 10; $CuCl_2$, 10; $CoCl_2$, 20; H_3BO_3, 10; Na_2MoO_4, 0.02 The pH was adjusted to 7.0 with HCl prior to filter sterilisation using a 0.2 μm filter (Sartorius).

S. coelicolor A3(2) strains were maintained on soy flour mannitol agar ($g\,l^{-1}$: soya flour, 20; mannitol, 20; agar, 16). Liquid cultures were prepared as follows. Spores stored in glycerol solution (50%, v/v) in cryotubes at −80 °C were used to inoculate 250 ml Erlenmeyer flasks containing 50 ml GG1 medium [11] which were incubated at 30 °C using triangular cross-section magnetic stirrer bars for agitation. After 48 h, 5 ml was removed from GG1 culture and used to inoculate 45 ml GYB medium [11] following the same incubation procedure (stirred 250 ml flasks) but for 24 h. After this, 20 ml GYB culture was used to inoculate sufficient 50 ml flasks of the P-limited defined medium, described above, to provide a 24 h inoculum culture at 10% (v/v) for bioreactor experiments.

2.2. Bioreactor culture

An Adaptive Biosystems Discovery bioreactor with a maximum working volume of 5 l was used. Agitation was provided by two disc turbine impellors rotating at 1000 rpm. Dissolved oxygen concentration in the bioreactor was monitored using a galvanic dissolved oxygen electrode (Uniprobe), and controlled by automatically varying the flow rate of sterile air through a sparger. The temperature was controlled at 30 °C. The pH was controlled to 6.80 by automatic addition of 1 M NaOH. Foaming was eliminated by including 0.001% Breox FMT30 antifoam (Water Management and Gamlen) in the culture medium.

Chemostat cultures were maintained at constant volume (1 l) with a weir overflow. The cultures were phosphate-limited and all other nutrients remained in excess throughout.

2.3. Enzyme activity

The activity of glucose-6-phosphate dehydrogenase was determined on freshly harvested samples according to the method of Scott and Cohen [14].

2.4. Culture supernatant analysis

Glucose was determined using an enzymatic kit (VWR International: 258264W). Ammonium was determined using a colorimetric assay kit (VWR International: 1.10024.0001). Phosphate was determined using a colorimetric assay kit (VWR International: 1.10428.0001). Nutrient concentrations were measured using an RQ-reflectoquant analyser (Merck/VWR International). Actinorhodin measurements were carried out using the method described by Bystrykh et al. [15]. Extracellular actinorhodin (i.e. in the supernatant) was analysed by placing 500 μl supernatant into a centrifuge tube to which a further 500 μl 3 M KOH was added. This was then vortexed and the absorbance measured at 640 nm using a Pharmacia Biotech Ultraspec 2000. If necessary, samples were diluted ensuring the same ratio of KOH to the supernatant was used. In the cultures where actinorhodin accumulated intracellularly, the pellet resulting from 20 ml sample was resuspended in 5 ml 3 M KOH. This suspension was sonicated (Heat Systems), on ice, for a total of 7 min (30 s on/off cycles). A further 15 ml 3 M KOH was then added and centrifuged. The process was repeated until no or negligible amounts of actinorhodin remained in the pellet. The absorbance of the supernatant was measured at 640 nm. The concentration of actinorhodin was calculated using a molar extinction coefficient (E_{640}) value of 25,320 $M^{-1}\,cm^{-1}$ [15].

2.5. Reproducibility and replication of experiments

All experimental data were obtained from single cultures. Experiments were carried out in triplicate to ensure that the trends and relationships observed in the culture parameters measured were reproducible. Individual assays were replicated four-fold. Experiments were rejected where a Chi squared test indicated significant differences between replicates.

2.6. Flux balance analysis

The genome scale model of *S. coelicolor* metabolism [5] was used for all metabolic simulations. These employed the flux balance analysis (FBA) approach [16,17]. The computational approaches were as described by Borodina et al. [5] except that the freeware GNU Linear Programming Kit (http://www.gnu.org/software/glpk/glpk.html) was used for linear optimisation.

3. Results and discussion

3.1. Effect of pIJ8714 insertion

The acquisition of the sequence changed actinorhodin production kinetics from growth dissociated (typical secondary metabolite) to growth associated production kinetics, in addition to increasing antibiotic yield (Fig. 1). These observations are consistent with reports describing so-called precocious antibiotic production, arising from the use of the constitutive *ermEp** promoter [18] to drive the pathway-specific activator gene *actII-ORF4*, and yield enhancement by adding an extra copy of *actII-ORF4* [19]. In these situations, the biosynthetic genes for actinorhodin biosynthesis are constitutively and highly expressed. Thus, M510(plJ8714) provided an ideal system for studying actinorhodin production in steady state chemostat culture in which secondary metabolite production is often low. This approach to strain construction also has significant generic potential for modifying commercially important *Streptomyces* and related

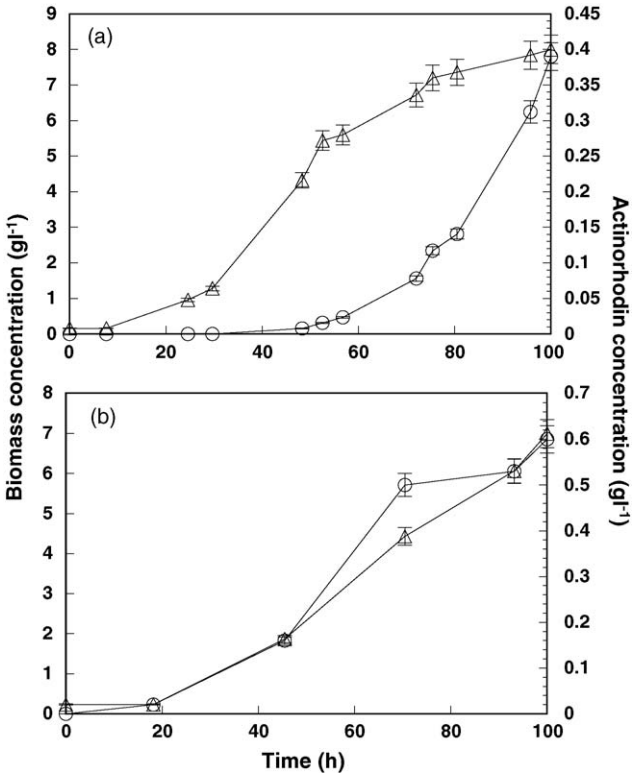

Fig. 1. Biomass (triangles) and actinorhodin (circles) concentrations as a function of time in bioreactor batch cultures of *Streptomyces coelicolor* M510 (a) and *S. coelicolor* M510(pIJ8714) (b).

strains for targeted specific over-expression of characteristics conducive to optimum bioreactor performance [19].

3.2. Effect of zwf mutation

Previous studies had shown that mutations in the glucose-6-phosphate dehydrogenase (*zwf*) gene could increase act production in *S. lividans* [11]. This was also shown to be the case in *S. coelicolor* batch culture (Table 1) when either one of the genes (*zwf*) coding for glucose-6-phosphate dehydrogenase in *S coelicolor* was deleted. Deletion of both genes resulted in a weakly viable phenotype in which no significant growth in liquid culture was obtained. Our mutants, therefore, differed from those in the *S. lividans* study [12] which involved *abolition* of glucose-6-phosphate dehydrogenase activity. Each of our single *zwf S. coelicolor* mutants exhibited increased *in vitro* glucose-6-phosphate dehydrogenase enzyme activity (Table 1). DNA microarray studies (data not shown) demonstrated that transcription of the remaining zwf gene also increased as a result of deletion of the other corresponding isogene. We are not aware of a precedent for the deletion of a gene coding for one of two isoforms resulting in enhanced activity of the corresponding remaining gene product. Perhaps, therefore, the increase in glucose-6-phosphate dehydrogenase activity is a result of disruption of cross-regulation at the transcriptional level, between the two isogenes.

Growth nutrient uptake and production of actinorhodin were measured in chemostat culture of M717(pIJ8714) (Δ*redD*, Δ*zwf1*). In the chemostat, it was possible to measure steady state production and consumption rates and it was found that the actinorhodin production rate increased approximately three-fold in the *zwf* mutant (Table 2).

3.3. Flux balance analysis

To examine the theoretical *in silico* effect of flux through the *zwf*-coded reaction on actinorhodin production, flux balance analysis [15,16] was carried out using the genome scale model of Borodina et al. [5] Setting a range of flux values through the glucose-6-phosphate dehydrogenase reaction as model bounds, and actinorhodin as the objective function, resulted in a predicted decrease in maximum theoretical actinorhodin production as glucose-6-phosphate dehydrogenase flux was increased (Fig. 2) when the model was constrained using observed glucose utilisation rates. The utilisation rates for nutrients that were absent from the defined medium were set to zero. As the *zwf* mutant exhibited a significantly increased phosphate uptake rate compared to the parental strain (Table 2) we also modelled the effect of varying the rate of phosphate consumption on theoretical maximum actinorhodin production. The predicted maximum actinorhodin production rate decreased linearly as the phosphate consumption rate increased, over the region of the model where predicted actinorhodin production rate was not significantly limited by glucose-6-phosphate dehydrogenase activity (Fig. 2).

3.4. Flux variability analysis

As our experimental results indicated that the M717(pIJ8714) (Δ*redD*, Δ*zwf1*) had increased *in vitro* glucose-6-phosphate dehydrogenase activity, coinciding with *increased* actinorhodin production rate and *increased* phosphate uptake rate (Table 2), the model was further constrained using observed phosphate and glucose uptake rates and actinorhodin production rates as bounding values. As carbon dioxide was not being used as a bounding

Table 1
Effect of *zwf* deletions on biomass and antibiotic productivity in P-limited batch culture

Strain (genotype)	Act_{max} ($\mu g\,ml^{-1}$)	Biomass $concn_{max}$ ($mg\,ml^{-1}$)	Specific act production ($mmol_{Act}\,g^{-1}_{biomass}$)	Percentage improvement compared to control strain (based on $\mu g_{Act}\,mg^{-1}_{biomass}$)
M510(pIJ8714) (Δ*redD*)	862	8.95	0.154	–
M717(pIJ8714) (Δ*redD*, Δ*zwf1*)	1090	7.36	0.243	58
M718(pIJ8714) (Δ*redD*, Δ*zwf2*)	1113	8.00	0.226	47

Act_{max} and Biomass $concn_{max}$ occurred at different times in the culture. Data for specific act production were obtained at the same time.

Table 2
Effect of *zwf* mutation on measured parameters in chemostat culture ($D = 0.04\ h^{-1}$)

Strain (genotype)	Act production rate (mmol $g_{biomass}^{-1}\ h^{-1}$)	Glucose consumption rate (mmol $g_{biomass}^{-1}\ h^{-1}$)	Phosphate consumption rate (mmol $g_{biomass}^{-1}\ h^{-1}$)	*In vitro* 6-P DH activity (mmol $g_{protein}^{-1}\ min^{-1}$)
M510(pIJ8714) (Δ*redD*)	0.00292	0.55506	0.01581	11.17
M717(pIJ8714) (Δ*redD*, Δ*zwf1*)	0.00870	0.52989	0.02124	20.17

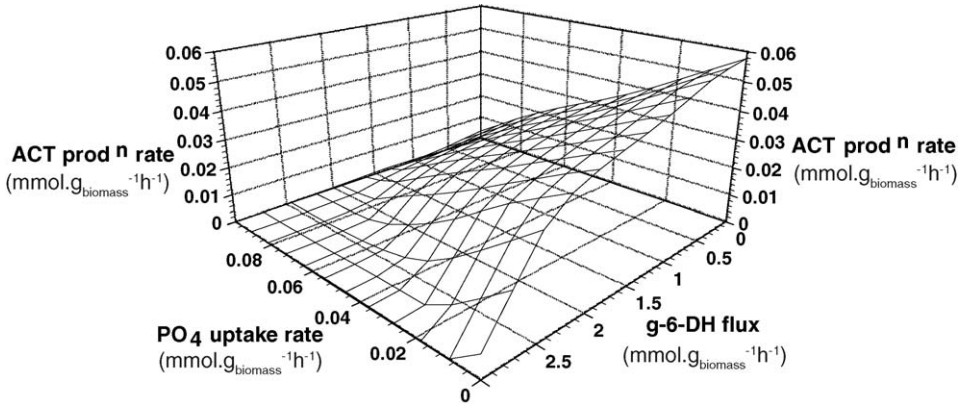

Fig. 2. Surface plot of the theoretical effect of varying phosphate uptake rate and flux through the glucose-6-phosphate dehydrogenase reaction on actinorhodin production using flux balance analysis of the genome scale metabolic network of Borodina et al. [5] assuming the availability only of nutrients present in the synthetic medium, and the experimentally observed glucose consumption rate of the M717(pIJ8714) (Δ*redD*, Δ*zwf1*) strain growing in chemostat culture.

Table 3
Reactions in the genome scale metabolic network ranked according to difference between flux range of each reaction in M510(pIJ8714) (Δ*redD*) and that of the corresponding reaction in M717(pIJ8714) (Δ*redD*, Δ*zwf1*)

EC no. (or gene)	Reaction	Pathway (Kegg classification)	Difference between flux range value for mutant and wild type (mmol $g\ h^{-1}$)
2.7.4.6	GDP + ATP = GTP + ADP	GTP/dGTP metabolism	3.125508
4.1.1.32	PEP + CO_2 + GDP = OA + GTP	Anaplerotic 4.1.1.32	3.125508
6.2.1.5	ADP + PI + SUCCOA = ATP + SUCC + COA	TCA cycle	3.069408
2.7.2.1	AC + ATP = ACETYLP + ADP	Pyruvate metabolism	3.069408
2.3.1.8	ACETYLP + COA = ACCOA + PI	Pyruvate metabolism	3.069408
1.1.1.37	MAL + NAD = NADH + OA	TCA cycle	2.625515
2.8.3.5	ACTAC + SUCCOA = SUCC + AACCOA	Butanoate metabolism	1.856532
2.7.1.40	PEP + ADP = PYR + ATP	Carbohydrate metabolism	1.810034
1.1.1.37	MAL + NAD = CO_2 + NADH + PYR	Pyruvate metabolism	1.810034
3.6.3.14	ADP + PI + 4H = ATP	Energy metabolism	1.753965
2.7.4.3	ATP + AMP = 2 ADP	ATP/dATP metabolism	1.753965
pith	PIint + H = PI	Proton-linked active transport	1.753965
6.2.1.16	ACTAC + ATP + COA = AACCOA + AMP + PPI	Leucine catabolism	1.753965
6.2.1.1	ATP + AC + COA = AMP + PPI + ACCOA	Pyruvate metabolism	1.753965
2.7.9.1	PYR + ATP + PI = PEP + AMP + PPI	Pyruvate metabolism	1.753965
pstB	PIint + ATP = 2PI + ADP	ABC transporter system	1.753965
3.6.1.1	PPI = 2PI + H	Energy metabolism	1.752092
1.3.3.1	DOROA + O_2 = H_2O_2 + OROA	Pyrimidine metabolism	1.595367
1.3.3.1	DOROA + MK = MKH2 + OROA	Pyrimidine metabolism	1.595367
6.4.1.2	ACCOA + ATP + CO_2 = MALCOA + ADP + PI	Pyruvate metabolism	1.520607
2.3.3.1	ACCOA + OA = COA + CIT	TCA cycle	1.464297
2.6.1.1	OA + GLU = ASP + AKG	Aspartate biosynthesis	1.441352
2.7.1.11	F6P + ATP = FDP + ADP	Fructose-6-phosphate phosphoryation	1.341692
1.4.1.13	AKG + GLN + NADH = NAD + 2 GLU	Glutamate biosynthesis	1.325919
1.4.4.4	AKG + NH_3 + NADPH = GLU + NADP	Glutamate biosynthesis	1.325914

Only the 25 highest values of the 700 reaction list are shown. There was an insignificant difference between flux variability of ammonia (0.622) and oxygen (0.271) uptake rates between the two strains. Example calculation for EC 2.7.4.6: minimum $flux_{M510} = -10.5926$; maximum $flux_{M510} = 7.133484$; $flux\ range_{M510} = 17.7261$. Minimum $flux_{M717} = -8.78095$; maximum $flux_{M717} = 5.819643$; $flux\ range_{M717} = 14.6005$. Flux range difference = 17.7261 − 14.6005 = 3.125508.

Table 4
Effect of 10 mM glutamate feeding on measured parameters in chemostat culture of M510(pIJ8714) (Δ*redD*) ($D = 0.04\ h^{-1}$)

Glutamate uptake rate (mmol $g_{biomass}^{-1}\ h^{-1}$)	Act production rate (mmol $g_{biomass}^{-1}\ h^{-1}$)	Glucose consumption rate (mmol $g_{biomass}^{-1}\ h^{-1}$)	Phosphate consumption rate (mmol $g_{biomass}^{-1}\ h^{-1}$)
0 (control)	0.00292	0.55506	0.01581
0.02	0.00346	0.31257	0.00862

value (model input), it was available as the objective function (model output), where its predicted value could be compared with observed experimental measurements.

One problem with flux balance analysis, as an approach to examining flux distribution, is that the intermediary fluxes, computed whilst optimising the objective function are not necessarily unique and, in most cases, a range of flux values for a particular reaction can result in the same objective function value. As a means of characterising the topology of the network, therefore, flux variability analysis [10] was performed on the genome scale model. The objective function (carbon dioxide production rate) was set to its optimal value and then the flux through each of the 700 reactions in the network was maximised and minimised [20]. The predicted maximum carbon dioxide production rates were similar to those observed experimentally for the two strains. All of the reactions in the model were ranked (Table 3) according to the magnitude of the difference between the flux value range in M717(pIJ8714) (Δ*redD*, Δ*zwf1*) and the corresponding reaction flux range in M510(pIJ8714) (Δ*redD*). In the ranking, those reactions whose predicted flux ranges had significantly narrowed

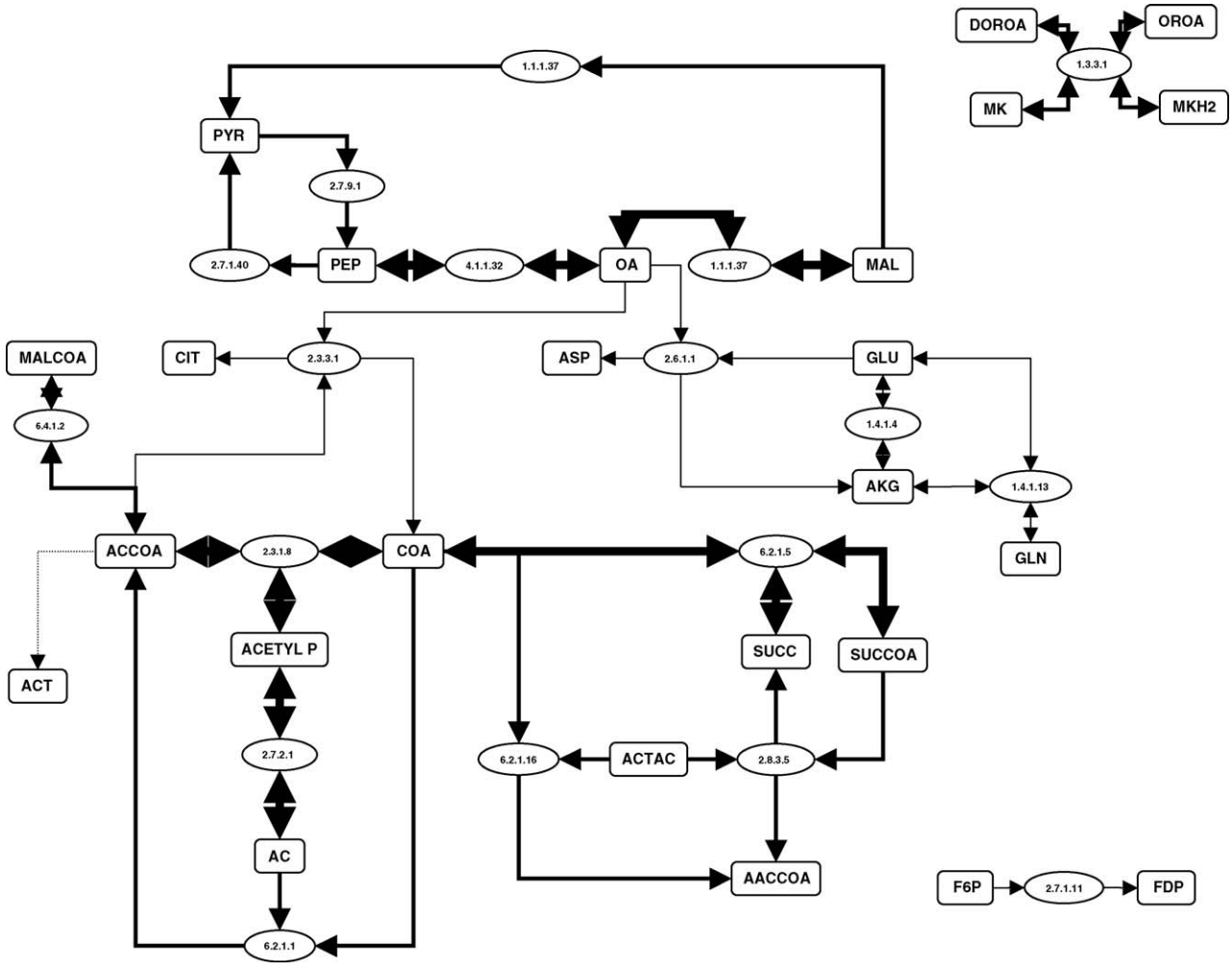

Fig. 3. Reactions with significantly reduced flux ranges in the genome scale model of M717(pIJ8714) (Δ*redD*, Δ*zwf1*) compared to the M510(plJ8714) (Δ*redD*) model, indicating their connectivity to each other and to actinorhodin biosynthesis. The weighting of the arrows indicates the degree to which the mutation has affected the flux variability of the reaction (heaviest weighting: 2–3 mmol $g^{-1}\ h^{-1}$; intermediate weighting: 1.5–2 mmol $g^{-1}\ h^{-1}$; lightest weighting: below 1.5 mmol $g^{-1}\ h^{-1}$. AC: acetate; ACCOA: acetyl Co A; AACCOA: acetoacetyl Co A; ACETYL P: acetyl phosphate; ACT: actinorhodin; ACTAC: acetoacetate; AKG: alpha ketoglutarate; ASP: aspartate; CIT: citrate; COA: Co A; F6P: fructose-6-phosphate; FDP: fructose-di-phosphate; GLN: glutamine; GLU: glutamate; MAL: malonate; MALCOA: malonyl Co A; MK: menaquinone; MKH2: menaquinone hydroquinone; OA: oxaloacetate; PEP: phosphoenolpyruvate; PYR: pyruvate; SUCC: succinate; SUCCOA: succinyl Co A.

Table 5
Reactions in the genome-scale metabolic network ranked according to difference between flux range of each reaction in M510(plJ8714) (Δ*redD*) and that of the corresponding reaction in M510(plJ8714) (Δ*redD*) using the observed glutamate uptake rate arising as a result of the glutamate feed

EC no. (or gene)	Reaction	Pathway (Kegg classification)	Difference between flux range value for non-fed and glutamate fed culture (mmol g h^{-1})
2.7.4.6	GDP + ATP = GTP + ADP	GTP/dGTP metabolism	11.46221
4.1.1.32	PEP + CO_2 + GDP = OA + GTP	Anaplerotic	11.46221
6.2.1.5	ADP + PI + SUCCOA = ATP + SUCC + COA	TCA cycle	11.00626
2.7.2.1	AC + ATP = ACETYLP + ADP	Pyruvate metabolism	11.00626
2.3.1.8	ACETYLP + COA = ACCOA + PI	Pyruvate metabolism	11.00626
1.1.1.37	MAL + NAD = NADH + OA	TCA cycle	9.639631
2.8.3.5	ACTAC + SUCCOA = SUCC + AACCOA	Leucine catabolism	6.749238
2.7.1.40	PEP + ADP = PYR + ATP	Carbohydrate metabolism	6.745258
1.1.1.37	MAL + NAD = CO_2 + NADH + PYR	Pyruvate metabolism	6.745258
3.6.1.1	PPI = 2PI + H	Energy metabolism	6.29174
3.6.3.14	ADP + PI + 4H = ATP	Energy metabolism	6.289268
pitH	PIint + H = PI	Proton-linked active transport	6.289268
6.2.1.16	ACTAC + ATP + COA = AACCOA + AMP + PPI	Leucine catabolism	6.289268
pstB	PIint + ATP = 2PI + ADP	ABC transporter system	6.289268
6.2.1.1	ATP + AC + COA = AMP + PPI + ACCOA	Pyruvate metabolism	6.289268
2.7.9.1	PYR + ATP + PI = PEP + AMP + PPI	Pyruvate metabolism	6.289268
2.7.4.3	ATP + AMP = 2ADP	ATP/dATP metabolism	6.289268
6.4.1.2	ACCOA + ATP + CO_2 = MALCOA + ADP + PI	Pyruvate metabolism	5.982683
1.3.3.1	DOROA + O_2 = H_2O_2 + OROA	Pyrimidine metabolism	5.883734
1.3.3.1	DOROA + MK = MKH2 + OROA	Pyrimidine metabolism	5.883734
2.6.1.1	OA + GLU = ASP + AKG	Aspartate biosynthesis	5.624877
2.3.3.1	ACCOA + OA = COA + CIT	TCA cycle	5.181218
2.7.1.11	F6P + ATP = FDP + ADP	Fructose-6-phosphate phosphoryation	4.957344
3.6.1.1	PPI = 2PI	Energy metabolism	4.718805
2.7.2.8	NAGLU + ATP = ADP + NAGLUP	Arginine biosynthesis	4.716997

Only the 25 highest values of the 700 reaction list are shown.

as a consequence of the changes in the bounding values, imposed by the *zwf* mutation were mostly those of pyruvate metabolism and the TCA cycle (Table 3) linked to acetylCoA, the precursor to actinorhodin biosynthesis in the model (Fig. 3).

The flux values of those reactions whose flux variabilities had been significantly reduced by the mutation could be regarded as having significant importance in modelling metabolism within the constraints imposed by the measured variables. As the measured variable that changed the most, as a result of the mutation, was actinorhodin production rate, it was assumed that changes in flux ranges resulted from redirection of metabolic flux towards production of this antibiotic. We propose that the magnitude of the reduction in the flux range of each reaction, as a result of increased actinorhodin production, is a potential measure of the influence of the flux value through that reaction on actinorhodin biosynthesis rate.

This modelling exercise identified some glutamate converting reactions as providing potential biosynthetic precursors for actinorhodin biosynthesis (Table 3, Fig. 5) and, in order to evaluate the possible applications of such analyses to process design, a glutamate feed was applied to the culture.

No significant changes in the flux range in reactions of the pentose phosphate pathway, including glucose-6-phosphate dehydrogenase, were predicted.

3.5. Effect of feeding glutamate

An 18% increase in actinorhodin production over that of the control was observed in the glutamate-fed cultures (Table 4).

Comparing the flux variabilities of the reactions in the glutamate fed culture, to those of the control (Table 5) highlighted the importance of the same reactions (with only two exceptions) as those identified above (Table 3, Fig. 3) in the network, using observed nutrient uptake values (including, in this case glutamate) and actinorhodin production rate as model bounds.

The elucidation of the physiological effect of the *zwf* mutation on antibiotic production requires further analysis, using ^{13}C tracer studies. Our *in vitro* enzyme assays, suggest that the mutation increased the activity of glucose-6-phosphate dehydrogenase *in vivo*. Increased actinorhodin biosynthesis rates cannot be achieved without increasing the rate of precursor (acetylCoA) production and our modelling studies have served to generate a hypothesis as to those reactions that are most likely to be involved. A simple process design, aimed at increasing flux through those reactions (initiating a glutamate feed) resulted in an increase in actinorhodin production rate and a consistent effect on the model.

4. Conclusions

Here, we report a number of novel findings. Deletion of one of the *zwf* homologues resulted in enhanced *in vitro* activity of the remaining gene product. Mutants carrying one of these deletions exhibited significantly increased actinorhodin biosynthesis. This effect could not have been predicted by simple flux balance simulation, constraining the model with glucose-6-phosphate dehydrogenase reaction flux values or phosphate uptake rate

with maximum actinorhodin production rate as the objective function. However, when the theoretical flux variability distribution, obtained using all experimental measured variables (including actinorhodin yield) as constraints, was examined, in the two strains (which differed only in the *zwf* mutation) a potential pivotal role for intracellular glutamate as an actinorhodin precursor was identified. Subsequent experiments, in which glutamate was fed to steady state cultures, resulted in increased actinorhodin production.

This study is an example of the possible role of constraints-based flux balance modelling in metabolic engineering. Since flux variability analysis defines a feasible range of fluxes for each individual reaction, no single flux value within each range can be considered unique. However, the limits of each range are unique values for the reaction concerned and, therefore provide a set of parameters for quantifying the solution space that describes the topology of the network. Flux variability analysis highlighted areas of metabolism from relatively disparate pathways that can be connected to form an actinorhodin-generating network.

Our previous studies [8,21] have demonstrated the use of rationally designed nutrient feeds for influencing antibiotic production rate. However, this is the first time that we have used a genome scale metabolic network for process design.

Acknowledgements

We thank BBSRC for provision of a research grant from the Engineering and Biological Systems committee. We are particularly grateful to Irina Borodina (Technical University of Denmark) for help and advice with implementing the genome scale metabolic network (which she developed), including the provision of expected values for diagnostic purposes.

References

[1] Borodina I, Nielsen J. From genomes to in silico cells via metabolic networks. Curr Opin Biotechnol 2005;16:350–5.
[2] Kauffman KJ, Prakash P, Edwards JS. Advances in flux balance analysis. Curr Opin Biotechnol 2003;14:491–6.
[3] Schilling CH, Edwards JS, Letscher D, Palsson BO. Combining pathway analysis with flux analysis for the comprehensive study of metabolic systems. Biotechnol Bioeng 2000;71:286–306.
[4] Bentley SD, Chater KF, Cerdeno-Tarraga AM, Challis GL, Thomson NR, James KD, et al. Complete genome sequence of the model actinomycete *Streptomyces coelicolor* A3(2). Nature 2002;417:141–7.
[5] Borodina I, Krabben P, Nielsen J. Genome-scale analysis of *Streptomyces coelicolor* A3(2). Genome Res 2005;15:820–8.
[6] Klamt S, Stelling J, Ginkel M, Gilles E. FluxAnalyzer: exploring structure, pathways, and flux distributions in metabolic networks on interactive flux maps. Bioinformatics 2003;19:261–9.
[7] Rozkov A, Avignone-Rossa CA, Ertl PF, Jones P, O'Kennedy RD, Smith JJ, et al. Characterization of the metabolic burden on *Escherichia coli* DH1 cells imposed by the presence of a plasmid containing a genetherapysequence. Biotech Bioeng 2004;88:909–15.
[8] Bushell ME, Kirk S, Zhao HJ, Avignone Rossa CA. Manipulation of the physiology of clavulanic acid biosynthesis with the aid of metabolic flux analysis. Enzyme Microb Technol 2006;39:149–57.
[9] Kirk S, Avignone-Rossa CA, Bushell ME. Growth limiting substrate affects antibiotic production and associated metabolic fluxes in *Streptomyces clavuligerus*. Biotech Lett 2000;22:1803–9.
[10] Reed JL, Palsson BO. Genome-scale in silico models of *E. coli* have multiple equivalent phenotypic states: assessment of correlated reaction subsets that comprise network states. Genome Res 2004;14:1797–805.
[11] Kieser T, Bibb MJ, Buttner MJ, Chater KF, Hopwood DA. Practical streptomyces genetics. Norwich, UK: John Innes Foundation; 2000.
[12] Butler MJ, Bruheim P, Jovetic S, Marinelli F, Postma PW, Bibb MJ. Engineering of primary carbon metabolism for improved antibiotic production in *Streptomyces lividans*. Appl Environ Microbiol 2002;68:4731–9.
[13] Bierman M, Logan R, O'Brien K, Seno ET, Nagaraja Rao R, Schoner. Plasmid cloning vectors for the conjugal transfer of DNA from *Escherichia coli* to *Streptomyces* spp. Gene 1992;116:43–9.
[14] Scott DBM, Cohen SS. The oxidative pathway of carbohydrate metabolism in *Escherichia coli*. 1. The isolation and properties of glucose 6-phosphate dehydrogenase and 6-phosphogluconate dehydrogenase. Biochem J 1959;55:23–33.
[15] Bystrykh LV, Fernandez Moreno MA, Herrema JK, Malpartida F, Hopwood DA, Dijkhuizen L. Production of actinorhodin-related "blue pigments" by *Streptomyces coelicolor* A3(2). J Bacteriol 1996;178:2238–44.
[16] Varma A, Palsson BO. Stoichiometric flux balance models quantitatively predict growth and metabolic by-product secretion in wild-type *Escherichia coli* W3110. Appl Environ Microbiol 1994;60:3724–31.
[17] Schilling CH, Edwards JS, Palsson BO. Toward metabolic phenomics: analysis of genomic data using flux balances. Biotechnol Prog 1999;15:288–95.
[18] Bibb MJ, Janssen GR, Ward JM. Cloning and analysis of the promoter region of the erythromycin resistance gene (*ermE*) of *Streptomyces erythraeus*. Gene 1985;38:215–26.
[19] Rowe CJ, Cortes J, Gaisser S, Staunton, Leadlay PF. Construction of new vectors for high-level expression in actinomycetes. Gene 1998;21:215–23.
[20] Mahadevan R, Schilling CH. The effects of alternate optimal solutions in constraint-based genome-scale metabolic models. Metab Eng 2003;5:264–76.
[21] Ives PR, Bushell ME. Manipulation of the physiology of clavulanic acid production in *Streptomyces clavuligerus*. Microbiology 1997;143:3573–9.